Material and Methods

Peptide Synthesis: All peptides were synthesized on solid support according to the procedure published by Carpino and Barlos for Fmoc-protected amino acids on TCP resin (PepChem, Tübingen, Germany).[1-4] N-Methylation of Fmoc-protected alanine was performed in solution according to the conditions described by Freidinger *et al*.[5] All the other N-methylated amino acids were obtained according to the optimized Mitsunobu conditions for N-methylation reported by Biron *et al*.[6, 7] While synthesizing the peptides on solid support, peptide couplings were performed using HOBT and TBTU for regular peptide couplings or HATU and HOAT for couplings after N-methylated amino acids. Treatment of the resin with 20% HFIP in DCM yielded the linear peptide. Cyclization was carried out using HATU and HOBt in DMF to give the crude cyclic peptide. The raw peptide was precipitated in brine followed by precipitation in water. The precipitated was redissolved in 95% TFA, 2.5% TIPS and 2.5% water and allowed to stir for 3h. Afterwards, the solution was concentrated under reduced pressure and the remaining solution added into ether. Finally, the obtained precipitated was purified via RP-HPLC.

NMR Spectroscopy: E.COSY, TOCSY, ROESY, 13C-HMBC, 13C-HSQC and a phase sensitive HMBC with selective 13C-pulses were recorded at 298 K on a Bruker Avance III spectrometer operating at 500 MHz. Samples were prepared in DMSO-d6 at concentrations of 10 mM in a 3 mm NMR tube. DMSO-d6 (1H at 2.52 ppm) was used as internal standard. Data were processed with Topspin 1.3 software from Bruker. The homo- and heteronuclear experiments E.COSY, TOCSY, ROESY, and magnitude mode ^{13}C-HMBC were performed with a spectral width of 11 ppm for ^{1}H and 195 ppm for ^{13}C. Individual phase sensitive HMBC spectra covering N-methyl and Val γ-methyl ^{13}C resonances (offset = 25 ppm, spectral width = 20 ppm) and backbone ^{13}C resonances (^{13}C offset = 172 ppm, spectral width = 8 ppm) were detected with a spectral width of 10 ppm for ^{1}H. The increments in t1 and t2 were adjusted to the information extracted from the individual experiments, ranging from 80 to 1433 increments in t1 and from 8192 to 32768 complex data points in t2. Depending on the individual experiments, 16 to 120 transients were averaged for each t1 value. A mixing time of 80 ms was used for TOCSY (spin lock field: 6.2 kHz; mixing sequence MLEV-17). The sequential assignment was obtained from heteronuclear J correlations that were extracted from HSQC and HMBC spectra. A compensated ROESY experiment, which was used for the extraction of inter proton distances, was performed with 150 ms mixing time and a spin lock field of 2.1 kHz.[8] The volume integrals of the individually assigned cross-peaks were compensated for offset effects and converted into distance constraints using the isolated spin pair approximation.[9] The ROESY cross-peak volumes were calibrated against the distance (2.81 Å) between the *N*Me D-Trp8 $H^{\varepsilon 1}$ and $H^{\zeta 2}$ protons. Upper and lower distance limits were set to plus and minus 10% of the calculated distances, respectively. For distance restraints referring to degenerate protons, the numbers n_1 and n_2 of the involved degenerate target protons were considered by multiplying the upper and lower bounds with a factor of $(n_1 n_2)^{1/6}$ as

multiplicity correction.[10] 0.4 Å were added on upper bounds as pseudoatom corrections for restraints referring to a methyl group. 0.8 Å were added on upper bounds as pseudoatom corrections for ROEs between two methyl groups. 10 intraresidual, 16 sequential interresidual and 7 non-sequential interresidual ROE derived distance restraints were used for structure calculations, with restraints between *N*Me-Ala^{6} and *N*Me-Phe^{11} counted as sequential.

$^{3}J_{HN\text{-}H\alpha}$ coupling constants were determined from 1D ^{1}H NMR spectra, $^{3}J_{H\alpha\text{-}H\beta}$ coupling constants from E.COSY and heteronuclear $^{3}J_{C'\text{-}H}$ coupling constants from phase sensitive HMBC spectra, using according reference signals.[11, 12]

Structure calculations for 7: The structural NMR refinement protocol included distance geometry (DG) calculations, energy minimizations, and molecular dynamics (MD) simulations. The DG program DISGEO was used to generate structures consistent with the 33 distance restraints derived from the ROEs.[13, 14] The DG procedure started with the embedding of 50 structures using random metrization. The structures obtained from DG were evaluated according to the lowest total restraint violations. Among 30 structures that were in best accordance with experimentally derived restraints, all had identical peptide backbone conformations.

The GROMACS 4.0 software package (www.gromacs.org)[15-17] was used to perform unrestrained MD calculations. Visualization of the simulation trajectories was performed using the software packages VMD[18] and SYBYL. The scripts g_cluster, g_dist and g_angle, that were used for analysis of the MD trajectory, were all packaged with GROMACS. The 53a6 united atom (CH, CH2 and CH3 groups represented as a single atom) forcefield, one of the GROMOS96 force fields,[19] was used for the molecular dynamic simulations. Temperature and pressure control was executed by Berendsen coupling.[20] Periodic boundary conditions were employed on a octahedral simulation box, which was built with a distance of 2 nm for the solute, that consisted of more than 1200 DMSO molecules. Cut off distances of 1.4 nm for electrostatic and Lennard-Jones non-bonding interactions were applied. Simulation time steps were set to 2 fs. Upon soaking of the box with DMSO, the system was equilibrated by an initial minimization and subsequent 50 ps MD simulations at 50, 100, 150, 200, 250 and 298 K using position restraints. At every single temperature a temperature and a pressure equilibration was performed. Within the individual MD steps, the temperature was gradually increased, while the force constants of the position restraints were decreased exponentially from 250000 KJmol^{-1}nm^{-2} at 50 K to 25 KJmol^{-1}nm^{-2} at 250° K. At 298 K no position restraints were applied. The final 50 ns MD simulation was carried out at 298° K. Coordinates were saved every 10 ps. As the applied forcefield does not explicitly take the covalent contribution of the observed strong hydrogen bonds into account, we compensated for that by applying one single distance restraint between Tyr^{7} H^{N} and Val10 H^{N}, during the MD simulation. This restraint was in well agreement with an experimentally derived ROE between these atoms. We further applied a dihedral angle restraint on Val^{10} χ_1 in order to keep this dihedral angle within the experimentally determined range.

Supplementary Results

Table S1. Resonance assignment of peptide **7** in DMSO-d6 at 298 K. Chemical shifts are referenced on DMSO (^{1}H at 2.520 ppm)

	H^N (H^{NMe})	H^α	H^β	H^γ	H^δ	H^ε	H^ζ	H^η
*N*Me-Ala6	(2.404)	4.772	0.228					
Tyr7	8.359	4.928	2.681 2.805		6.949	6.698		9.273
*N*Me-D-Trp8	(2.886)	5.188	proR: 3.184 proS: 2.915		1: 7.136	1: 10.960 3: 7.449	2: 7.410 3: 7.105	2: 7.144
*N*Me-Lys9	(2.506)	4.873	1.153 1.848	0.669 0.872	1.405	2.705	7.683	
Val10	6.995	4.891	2.142	proR:0.833 proS:0.774				
*N*Me-Phe11	(3.210)	5.295	3.080 3.140		7.254	7.315	7.258	

Table S2. Comparison between the experimentally derived distance restraints (d_{low}), (d_{upp}) and calculated (d_{MD}) interproton distances of compound **7** as obtained from restrained MD calculation (r^{-6} averaged distance as backcalculated from the 50 ns MD trajectory). Violations of upper bounds (positive sign) and of lower bounds (negative sign) are given in the last column (d_{viol}).

interproton distance		d_{low} [Å]	d_{upp} [Å]	d_{MD} [Å]	d_{viol} [Å]
*N*Me-Ala^6 H^{Me}	*N*Me-Ala^6 H^α	3.60	4.81	3.59	-0.01
*N*Me-Ala^6 H^{Me}	*N*Me-Ala^6 H^β	3.19	4.69	3.49	
*N*Me-Ala^6 H^α	Tyr^7 H^N	2.18	2.66	2.32	
*N*Me-Ala^6 H^β	Tyr^7 H^N	4.11	5.42	4.28	
*N*Me-Ala^6 H^{Me}	Tyr^7 H^N	3.04	4.11	3.90	
*N*Me-Ala^6 H^{Me}	Tyr^7 H^α	4.40	5.78	5.40	
*N*Me-Ala^6 H^α	*N*Me-d-Trp^8 H^{Me}	4.50	5.90	5.37	
*N*Me-Ala^6 H^{Me}	Val^{10} $H^{\gamma2}$	4.27	6.02	6.33	+0.31
*N*Me-Ala^6 H^α	*N*Me-Phe^{11} H^α	1.61	1.96	1.61	
*N*Me-Ala^6 H^{Me}	*N*Me-Phe^{11} H^α	4.61	6.03	4.26	-0.35
Tyr^7 H^N	*N*Me-D-Trp^8 H^α	4.08	4.99	4.74	
Tyr^7 H^N	*N*Me-D-Trp^8 H^{Me}	3.89	5.15	4.18	
Tyr^7 H^α	*N*Me-D-Trp^8 H^{Me}	2.28	3.18	2.45	
Tyr^7 H^N	Val^{10} H^N	2.82	3.44	3.31	
Tyr^7 H^N	Val^{10} $H^{\gamma2}$	2.99	4.06	4.26	+0.20
Tyr^7 H^N	*N*Me-Phe^{11} H^{Me}	5.01	6.52	5.11	
*N*Me-d-Trp^8 H^α	Val^{10} H^N	3.19	3.90	3.59	
*N*Me-d-Trp^8 H^α	Val^{10} $H^{\gamma2}$	4.61	6.04	5.03	
Val^{10} H^N	Val^{10} H^β	3.28	4.01	3.64	
Val^{10} H^α	Val^{10} H^β	2.06	2.52	2.35	
Val^{10} H^N	Val^{10} $H^{\gamma1}$	3.39	4.55	3.65	
Val^{10} H^α	Val^{10} $H^{\gamma1}$	2.61	3.59	2.81	
Val^{10} H^N	Val^{10} $H^{\gamma2}$	2.70	3.70	2.92	
Val^{10} H^α	Val^{10} $H^{\gamma2}$	3.53	4.72	3.70	
Val^{10} H^N	*N*Me-Phe^{11} H^α	4.25	5.19	4.59	
Val^{10} H^α	*N*Me-Phe^{11} H^{Me}	2.21	3.10	2.45	
Val^{10} H^β	*N*Me-Phe^{11} H^{Me}	2.38	3.31	3.59	+0.28
Val^{10} $H^{\gamma2}$	*N*Me-Phe^{11} H^{Me}	4.43	6.21	5.47	
Val^{10} $H^{\gamma1}$	*N*Me-Phe^{11} H^{Me}	4.43	6.22	4.96	
*N*Me-Phe^{11} H^α	*N*Me-Phe^{11} H^{Me}	3.44	4.60	3.11	-0.33

Table S3. Average Φ and Ψ dihedral angles and their standard deviations as extracted from the MD trajectory.

Amino acid residue	Φ_{MD} [°]	Ψ_{MD} [°]
N-Me-Ala6	-122.8 +/- 6.6	67.9 +/- 21.5
Tyr7	-132.7 +/- 19.2	114.9 +/- 13.1
N-Me-D-Trp8	81.1 +/- 11.4	-107.2 +/- 8.1
N-Me-Lys9	-111.6 +/- 12.0	0.8 +/- 22.1
Val10	-117.4 +/- 18.3	120.8 +/- 14.0
N-Me-Phe11	-44.7 +/- 24.7	115.6 +/- 9.4

Table S4. $^3J_{H\alpha\text{-}H\beta}$ Coupling Constants and the according χ_1 populations, as derived by assuming the following coupling constants: $^3J_{H\alpha\text{-}H\beta}(ap) = 12$ Hz, $^3J_{H\alpha\text{-}H\beta}(ga) = 3.5$ Hz.

	$^3J_{H\alpha\text{-}H\beta}$ [Hz]		p(χ_1 = -60°) [%]	p(χ_1 = 180°) [%]	p(χ_1 = 60°) [%]
	H^α-H^β proR	H^α-H^β proS			
Tyr7	4.5, 7.1		54		46
N-Me-D-Trp8	10.5	5.8	0	78	22
N-Me-Lys9	11.0, 4.7		100		0
Val10	4.0		94	6	0
N-Me-Phe11	5.8, 10.6		100		0

Side chain structure and dynamics: Investigation of side chain conformation about the χ_1 angle requires a careful analysis of homo- and heteronuclear J couplings as well as the consideration of NOE distances in stereospecifically assigned β protons.[21] Extended MD simulations of a solution structure in explicit solvent can further clarify which structural flips of side chain dihedral angles are correlated.

The sums of the $^3J_{H\alpha\text{-}H\beta}$ coupling constants of the residues *N*Me-D-Trp[8], *N*Me-Lys[9] and *N*Me-Phe[11] exceed 15 Hz, which excludes higher populations of the $\chi_1 = 60°$ conformation (gauche-) for the *N*Me-D-Trp[8] residue, and of the $\chi_1 = -60°$ conformation (gauche+) for the *N*Me-Lys[9] and *N*Me-Phe[11] residues (Table S4). The sum of the Tyr[7] $^3J_{H\alpha\text{-}H\beta}$ coupling constants (12.6 Hz) is significantly smaller and indicates a considerable population of the χ_1=60° rotamer, that is for steric reasons usually disfavored in L amino acid residues. A small $^3J_{H\alpha\text{-}H\beta}$ coupling constant of 4.0 Hz excludes the Val[10] χ_1=180° rotamer (with antiperiplanar orientation of H^α and H^β) from being populated significantly. A strong difference between the two $^3J_{H\alpha\text{-}H\beta}$ coupling constants together with a sum of both of more than 15 Hz indicate a preferred (χ_1=180°) conformation for *N*Me-D-Trp[8] ($^3J_{H\alpha\text{-}H\beta proR}$ = 10.5 Hz), whereas signal overlap or a poor signal to noise ratio precluded similar unambiguous stereospecific assignments and a similar detailed analysis of χ_1 populations of the other non β branched residues. Consideration of the intraresidual Val[10] H^N-H^{Me} and H^α-H^{Me} ROEs together with the small $^3J_{H\alpha\text{-}H\beta}$ coupling constant (4.0 Hz) and the large $^3J_{HN\text{-}H\alpha}$ constant (9.3 Hz) clearly demonstrated a very strong

preference of χ_1 = -60° for this residue. Overall, the $^3J_{H\alpha\text{-}H\beta}$ coupling constants agree well with χ_1 rotamer populations that were observed in the MD simulation (Figure S1).

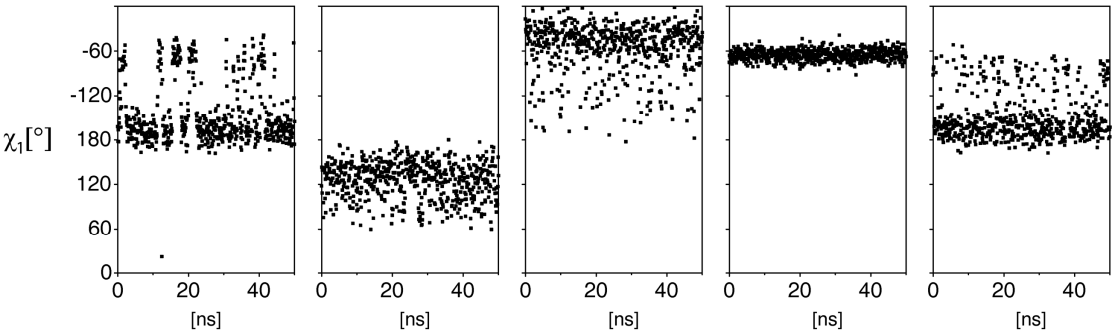

Figure S1. χ_1 dihedral angles as observed during 50 ns MD simulation from residue Tyr7 on the left in sequential order to residue *N*-Me-Phe11 on the right.

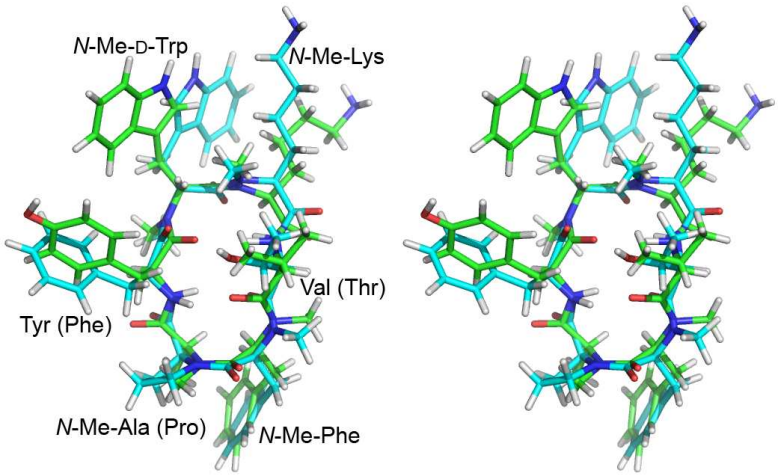

Figure S2. Overlay of the solution structure of peptide **7** with the structure of the similar threefold *N*-methylated cyclo(-PFMewMeKTMeF-).[22] In positions that are occupied by different residues within the two peptides, residues of cyclo(-PFMewMeKTMeF-) are given in brackets. The root mean squared deviation of the peptide backbones is 0.55 Å.

Analytical data

MK678_0:

HPLC: tR(C18 column 10-100% ACN:H2O+ 0.1% TFA): 15.15 min

ESI-MS: Mol Wt. $(M+H)^+$: 809.4

MK678_1:

HPLC: tR(C18 column 10-100% ACN:H2O+ 0.1% TFA): 15.91 min

ESI-MS: Mol Wt. $(M+H)^+$: 823.4

MK678_2:

HPLC: tR(C18 column 10-100% ACN:H2O+ 0.1% TFA): 15.81 min

ESI-MS: Mol Wt. $(M+H)^+$: 823.5

MK678_3:

HPLC: tR(C18 column 10-100% ACN:H2O+ 0.1% TFA): 16.13 min

ESI-MS: Mol Wt. $(M+H)^+$: 823.4

MK678_4:

HPLC: tR(C18 column 10-100% ACN:H2O+ 0.1% TFA): 16.87 min

ESI-MS: Mol Wt. $(M+H)^+$: 837.4

MK678_5:

HPLC: tR(C18 column 10-100% ACN:H2O+ 0.1% TFA): 17.12 min

ESI-MS: Mol Wt. $(M+H)^+$: 837.5

MK678_6:

HPLC: tR(C18 column 10-100% ACN:H2O+ 0.1% TFA): 16.70 min

ESI-MS: Mol Wt. $(M+H)^+$: 837.5

MK678_7:

HPLC: tR(C18 column 10-100% ACN:H2O+ 0.1% TFA): 17.83 min

ESI-MS: Mol Wt. $(M+H)^+$: 851.5

References

[1] K. Barlos, O. Chatzi, D. Gatos, G. Stavropoulos, *Int J Pept Protein Res* **1991**, *37*, 513.

[2] K. Barlos, D. Gatos, J. Kallitsis, G. Papaphotiu, P. Sotiriu, Y. Wenging, W. Schäfer, *Tetrahedron Letters* **1989**, *30*, 3943.

[3] L. A. Carpino, G. Y. Han, *J. Org. Chem.* **1972**, *37*, 3404.

[4] L. A. Carpino, D. Sadat-Aalaee, H. G. Chao, R. H. DeSelm, *J. Am. Chem. Soc.* **1990**, *112*, 9651.

[5] R. M. Freidinger, J. S. Hinkle, D. S. Perlow, B. H. Arison, *J. Org. Chem.* **1983**, *48*, 77.

[6] E. Biron, H. Kessler, *J. Org. Chem.* **2005**, *70*, 5183.

[7] E. Biron, J. Chatterjee, H. Kessler, *J. Pept. Sci.* **2006**, *12*, 213.

[8] C. Griesinger, R. R. Ernst, *J. Magn. Reson.* **1987**, *75*, 261.

[9] A. Kumar, G. Wagner, R. Ernst, K. Wüthrich, *J. Am. Chem. Soc.* **1981**, *103*, 3654.

[10] D. Neuhaus, M. Williamson, *The nuclear Overhauser effect in structural and conformational analysis*, second ed., John Wiley & Sons, **2000**.

[11] M. Eberstadt, G. Gemmecker, D. F. Mierke, H. Kessler, *Angew. Chem., Int. Ed.* **1995**, *34*, 1671.

[12] J. J. Titman, D. Neuhaus, J. Keeler, *Journal of Magnetic Resonance* **1989**, *85*, 111.

[13] D. F. Mierke, H. Kessler, *Biopolymers* **1993**, *33*, 1003.

[14] T. F. Havel, *Prog. Biophys. Mol. Biol.* **1991**, *56*, 43.

[15] E. Lindahl, B. Hess, D. van der Spoel, *Journal of Molecular Modelling* **2001**, *7*, 306.

[16] D. van der Spoel, E. Lindahl, B. Hess, G. Groenhof, A. E. Mark, H. J. C. Berendsen, *Journal of Computational Chemistry* **2005**, *26*, 1701.

[17] D. van der Spoel, E. Lindahl, B. Hess, A. R. van Buuren, P. J. Apol, P. J. Meulenhoff, D. P. Tieleman, A. L. T. M. Sijbers, K. A. Feenstra, R. van Drunen, H. J. C. Berendsen, *Gromacs User Manual version 4.0*, **2005**.

[18] W. Humphrey, A. Dalke, K. Schulten, *J. Mol. Graph.* **1996**, *14*, 33.

[19] W. F. van Gunsteren, S. R. Billeter, A. A. Eising, P. H. Hünenberger, P. Krüger, A. E. Mark, W. R. P. Scott, I. G. Tironi, *Biomolecular simulation: the GROMOS96 manual and user guide, 1st ed.*, Hochschulverlag AG an der ETH Zürich, Zürich, **1996**.

[20] H. J. C. Berendsen, J. P. M. Postma, W. F. van Gunsteren, A. DiNola, J. R. Haak, *Journal of Chemical Physics* **1984**, *81*, 3684.

[21] H. Kessler, C. Griesinger, K. Wagner, *J. Am. Chem. Soc.* **1987**, *109*, 6927.

[22] E. Biron, J. Chatterjee, O. Ovadia, D. Langenegger, J. Brueggen, D. Hoyer, H. A. Schmid, R. Jelinek, C. Gilon, A. Hoffman, H. Kessler, *Angew Chem Int Ed Engl* **2008**, *47*, 2595.